

Generation of high-energy electron-positron beams in the collision of a laser-accelerated electron beam and a multi-petawatt laser

M. Lobet,^{1,2,*} X. Davoine,^{1,†} E. d'Humières,² and L. Gremillet^{1,‡}

¹CEA, DAM, DIF, F-91297, Arpajon, France

²CELIA, UMR 5107, Université de Bordeaux-CNRS-CEA, 33405, Talence

Generation of antimatter via the multiphoton Breit-Wheeler process in an all-optical scheme will be made possible on forthcoming high-power laser facilities through the collision of wakefield-accelerated GeV electrons with a counter-propagating laser pulse with $10^{22} - 10^{23} \text{ Wcm}^{-2}$ peak intensity. By means of integrated 3D particle-in-cell simulations, we show that the production of positron beams with $0.05 - 1 \text{ nC}$ total charge, $100 - 400 \text{ MeV}$ mean energy and $0.01 - 0.1 \text{ rad}$ divergence is within the reach of soon-to-be-available laser systems. The variations of the positron beam's properties with respect to the laser parameters are also examined.

Introduction - The generation of dense positron beams is of great interest in many research areas, encompassing fundamental science [1], accelerator physics [2], material analysis [3] and laboratory astrophysics [4]. In the latter field, a driving goal is to understand the formation and dynamics of the electron-positron (e^-e^+) pair plasmas involved in a number of powerful space environments (pulsar winds, gamma-ray bursts, active galactic nuclei) [5]. The laboratory reproduction of these phenomena is hampered by the need to create pair plasmas dense enough to trigger collective effects. The use of ultra-intense, short-pulse lasers provides a promising path to this objective, as testified by the various schemes put forward in recent years [6–11]. The experimental studies carried out so far exclusively rely upon the Bethe-Heitler conversion of bremsstrahlung γ -rays emitted by energetic electrons injected through thick ($\sim \text{cm}$) high- Z targets. These electrons are produced either by direct irradiation of the converter target by an intense ($\sim 10^{20} \text{ Wcm}^{-2}$) picosecond laser [6] or by a few-femtosecond laser wakefield accelerator [7], in both cases leading to record positron densities of $\sim 10^{16} \text{ cm}^{-3}$.

The coming into operation of multi-PW lasers (e.g., the CILEX-Apollon [12] and ELI [13] facilities) expected to reach intensities $\sim 10^{23} \text{ Wcm}^{-2}$, should make it possible to investigate alternative concepts of pair generation, based on the Breit-Wheeler decay of γ -rays produced by nonlinear Compton scattering [9, 14]. Theory and simulations predict that quasi-neutral, high-density ($> 10^{21} \text{ cm}^{-3}$) relativistic pair plasmas could be generated from gas jets or thin solid foils [15, 16], through pair cascading from seed electrons or photons [10, 17–19], or using the flying-mirror concept [20]. In the near future, however, the most accessible route to laser-driven Breit-Wheeler pair production will exploit the collision of relativistic electrons with counter-propagating high-power lasers [21–23]. This concept was demonstrated two decades ago at SLAC by making a 46 GeV electron beam interact with a 10^{18} Wcm^{-2} laser [24], and is planned to be reproduced at higher electron energies on the future linear collider [25]. An all-optical scheme,

based on a laser wakefield accelerator (LWFA) instead of a conventional accelerator, should be within the reach of multi-PW, multi-beam laser systems. As a first step, consistently with theoretical predictions [26–30], recent state-of-the-art experiments have confirmed the potential of this configuration for generating high-brilliance γ -ray photon beams [31]. In order to provide guidelines for future experiments, we present in this Letter the first integrated, one-to-one simulation study of the pair production expected on the upcoming multi-PW laser facilities. Focusing on interaction conditions accessible to the CILEX-Apollon system [12], we characterize in detail the generated e^-e^+ beam and examine the sensitivity of its properties to the laser parameters.

Simple estimates of pair production - We start by estimating the efficiency of pair production during the head-on collision of a relativistic electron beam with an intense laser by means of a reduced kinetic quantum electrodynamic (QED) model [22, 32, 33]. This model describes the time evolution of the electron, positron and photon energy distributions under the action of a counter-propagating laser plane wave, taking into account the nonlinear Compton scattering and Breit-Wheeler pair creation. Unidirectional propagation of the particles at the speed of light is assumed, while advection and collective effects are neglected. Figures 1(a,b) display, as a function of the laser intensity (I_0) and the electron beam energy (ε_-), the predicted number of photons (of energies $\varepsilon_\gamma > 2m_e c^2$, where m_e is the electron mass) and positrons created per beam electron and per laser period. In the case of a LWFA driven by the 1-PW laser pulse of the CILEX-Apollon system ($0.8 \mu\text{m}$ wavelength, 15 J energy, 30 fs FWHM duration, $23 \mu\text{m}$ FWHM spot size), we expect from Lu's model [34] an initial beam energy $\sim 2 \text{ GeV}$ for a total charge $\sim 1 \text{ nC}$. The beam is then made to collide head-on with the CILEX-Apollon 5-PW, 15 fs laser pulse, focused to a maximum intensity of 10^{23} Wcm^{-2} . Our calculation indicates that each beam electron will produce approximately 20 γ -ray photons and $0.5 e^-e^+$ pair. The interaction will thus yield a positron beam of total charge close to that of the incident electron beam,

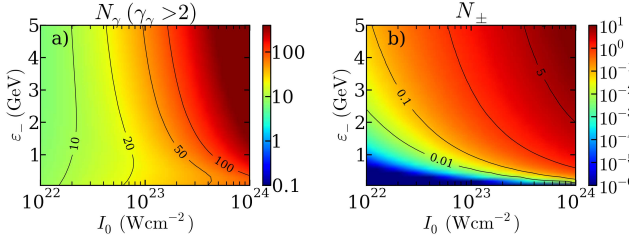


FIG. 1. Reduced kinetic-QED calculation: number of γ -ray photons (of energies $\varepsilon_\gamma > 2m_e c^2$) (a) and positrons (b) produced per laser period in the collision of a beam electron with a counter-propagating laser wave, as a function of the electron energy and the laser intensity. Countour lines are shown as black curves.

and of several hundred MeV average energy (not shown), comparable to the average photon energy.

Integrated kinetic simulations - For a more accurate description of the pair production, we make use of two complementary particle-in-cell (PIC) codes. The laser wakefield acceleration is simulated by means of the quasi-axisymmetric code CALDER-CIRC [35], based on a reduced cylindrical discretization of the Maxwell equations, which allows for handling of the spatio-temporal scales of the problem at a reduced computational cost. The resulting electron beam is then transferred to the three-dimensional (3D) Cartesian code CALDER [36], enriched with Monte Carlo models of the photon and pair production [33].

Electron acceleration with the Apollon 1-PW laser - In a first stage, we simulate the wakefield acceleration induced by the Apollon 1-PW laser (the parameters of which are given above). We first consider a 1.5 cm-long, flat plasma profile with a density of $0.0016n_c$ (n_c is the critical density at $1\mu\text{m}$). In good agreement with Lu's scaling laws [34], we obtain a 2-GeV electron bunch accompanied by a broad low-energy tail, with a total beam charge of 5 nC. In order to boost the beam energy, which is a key parameter for pair creation, we resort to a two-step plasma profile, comprising a 6.3 mm-long plateau at $0.0016n_c$ followed by a 5.6 mm-long plateau at $0.0032n_c$. This density jump aims at narrowing the plasma bubble when the trapped electrons approach their dephasing length, hence relocating them in the highest accelerating region of the wakefield, at the back of the bubble. This selects the beam head, increasing its energy up to 3.8 GeV, while reducing its charge to ~ 2 nC. The increased monochromaticity of the whole electron beam (above 100 MeV) is clearly seen in the phase space of Fig. 3(a) and the energy spectrum of Fig. 3(e). It is found that 63% of the total beam charge is contained in the beam head (between 2.5 and 3.8 GeV). The rest is mostly carried by a secondary electron bunch (with energies under 1.7 GeV) resulting from self-injection in the shortened bubble. The beam has an average diver-

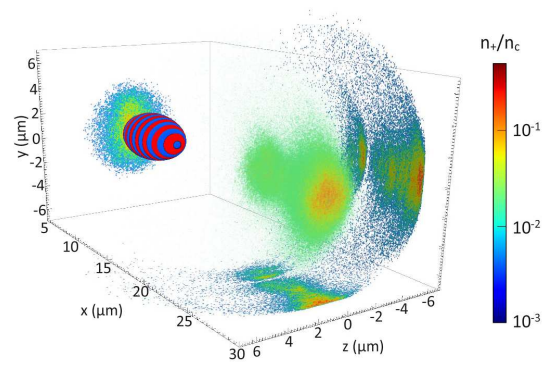


FIG. 2. Positron density isosurfaces at $t = 32$ fs after the laser peak. Density slices along the $x = 27.5\mu\text{m}$ (corresponding to the denser part of the beam head), $y = 0$ and $z = 0$ planes are projected onto the yz , xz and xy domain boundaries, respectively. The laser is represented through isosurfaces of the normalized electric field ($eE_y/m_e c\omega_0 = \pm 100$).

gence of 3 mrad, transverse FWHM sizes of $4\mu\text{m}$ and $2\mu\text{m}$ FWHM respectively along and normal to the laser polarization direction (y -axis), and a longitudinal length of $12\mu\text{m}$.

Pair generation during the collision with the 5-PW laser - The electron beam is then made to collide head-on with the CILEX-Apollon 5-PW laser. The pulse parameters (15 fs duration, $2\mu\text{m}$ focal spot) are chosen so as to reach a maximum intensity of 10^{23} Wcm^{-2} at the beam head. Consistently with our simple estimates, the laser-beam interaction is strong enough to cause copious pair production, as depicted in Fig. 2. During the collision, 85 % of the beam energy is radiated in the form of a broad photon distribution [solid green line in Fig. 3(e)] extending from hard x-rays to γ -rays, with a maximum energy of 3.5 GeV, close to the maximum electron energy, and an average energy of 33 MeV. Around this energy, the forward-directed photons present an angular divergence of ~ 3 mrad (equal to the beam's), yielding an approximate brilliance of $\sim 5 \times 10^{23}\text{ photons s}^{-1}\text{ mm}^{-2}\text{ mrad}^{-2}$ 0.1% BW, three orders of magnitude larger than the current experimental record [31].

Figure 2 shows that pair production is maximal at the beam head where the tightly focused pulse encounters the most energetic electrons. The e^-e^+ pairs carry $\sim 5\%$ of the incident electron beam energy, with a total positron charge $Q_+ \sim 0.8\text{ nC}$ amounting to $\sim 38\%$ of the initial beam charge. As predicted by the reduced QED model, the pulse intensity is too low to achieve global quasi-neutrality (*i.e.*, the production of more than a pair per incident electron). Yet, at the end of the interaction, most of the incident electrons have been expelled by the laser out of the central pair-filled region, so that the local positron density $n_+ \sim 0.13n_c$ (averaged over

the transverse $\sim 1 - 2 \mu\text{m}$ FWHM at the beam head) makes up for a significant fraction ($\sim 40\%$) of the total leptonic density ($n_- + n_+ \sim 0.32n_c$). The pair generation process is detailed in Figs. 3(a-d). Radiative losses become strong (associated with a quantum parameter [14] $\chi_- \sim 5 \times 10^{-6} a_0 \gamma_- \gtrsim 0.1$, where a_0 is the normalized wave vector and γ_- the electron Lorentz factor) as soon as the GeV electrons experience a laser intensity $\gtrsim 10^{21} \text{ Wcm}^{-2}$. Figure 3(b) shows that the beam head electrons have lost more than 90% of their initial energy by the time they see the laser maximum. Following the interaction, the electron beam spectrum is strongly broadened towards lower energies, with an average energy of $\sim 190 \text{ MeV}$ [Fig. 3(e), blue curves]. The relatively large value of the maximum energy ($\sim 3.2 \text{ GeV}$) corresponds to off-axis electrons weakly interacting with the laser field. This maximum energy is found to drop to 1.5 GeV for a laser plane wave of the same intensity and duration (not shown).

From comparison of the photon spectra at birth and after the collision [Fig. 3(e), green curves], we find that pair production mainly arises from photons of energy $\gtrsim 0.5 \text{ GeV}$. These photons have a decay length close to the pulse length, and they are produced in large numbers only during a few periods before the intensity peak [Fig. 3(c)].

The e^-e^+ pairs are created with a broad energy distribution (from $\sim 10 \text{ MeV}$ to 3 GeV), associated with an average value $\sim 0.5 \text{ GeV}$ [Fig. 3(e), dashed blue curve]. However, while subsequently moving through the remaining part of the pulse, they undergo significant radiative losses and the emitted photons can in turn trigger a short-duration pair cascade. At the end of the interaction, about 4.5 % of the total positron number originates from cascading, while the positron spectrum is strongly shifted to the low-energy side, with a much reduced mean energy $\sim 110 \text{ MeV}$ [Fig. 3(e), solid blue curve].

The final angular spread of the positron beam ($\theta_{+,xy}^f \sim 0.33 \text{ rad}$ and $\theta_{+,xz}^f \sim 0.2 \text{ rad}$ in the laser polarization and perpendicular planes, respectively) exceeds by two orders of magnitude that of the incident electrons ($\sim 0.003 \text{ rad}$), and it is also significantly larger than the angular spread of the positrons at birth ($\theta_{+,xy}^0 \sim 0.014 \text{ rad}$ and $\theta_{+,xz}^0 \sim 0.001 \text{ rad}$). Moreover, it appears to be close to the final divergence of the electron beam ($\theta_{-,xy} \sim \theta_{-,xz} \sim 0.3 \text{ rad}$). As for the electrons, the increase in the positron angular spread during the laser interaction has two possible origins. First, in the quantum radiation reaction regime considered here, photon emission in the laser field goes along with strong angular scattering, even in the plane-wave case [37]. This deflection mainly takes place in the xy laser polarization plane: as time increases, the radiating particles progressively lose x -momentum while their y -momentum saturates at a value $p_y \propto a_0$ after a few laser cycles [37, 38]. This feature starkly contrasts with classical radiation reaction,

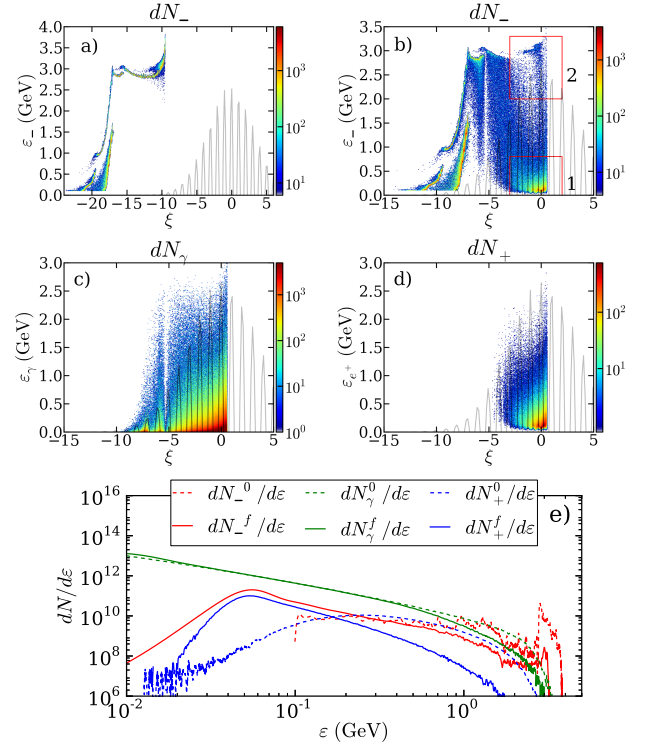


FIG. 3. (a,b) Electron energy spectra (transversely averaged) before (a) and during (b) the laser-beam collision as a function of the distance $\xi = [x - x_p(t)]/\lambda_0$ from the laser peak. In panel (b), frame 1 locates the on-axis beam head after strong radiative deceleration in the rising part of the laser, while frame 2 corresponds to the beam electrons traveling outside of the laser focus. (c) Photon and (d) positron energy spectra (transversely averaged) at the time of panel (b). In panels (a-d), the gray line plots the laser $|E_y|$ profile. (e) Integrated energy spectra of the electrons (blue), photons (green) and positrons (green) before ($dN^0/d\varepsilon$, dashed lines) and after ($dN^f/d\varepsilon$, solid lines) after the laser-beam collision

through which a particle cannot gain transverse momentum from a plane wave. Second, the particles can be deflected by the transverse ponderomotive force associated with the small laser spot size. Contrary to the quantum photon emission, which increases the transverse particle momentum only along the polarization y -axis, the ponderomotive force acts along both the y - and z -axes. The observed close variations of θ_{xy} and θ_{xz} during the interaction for both the positrons and electrons thus demonstrate that ponderomotive and QED effects become comparable under the present conditions (even though QED scattering still dominates for the positrons). One should note, however, that the important radiative deceleration in the x -direction amplifies the ponderomotive-driven angular deflection.

Influence of the laser parameters - We now examine how the laser parameters affect the positron production. To this goal, we have performed four laser-electron colli-

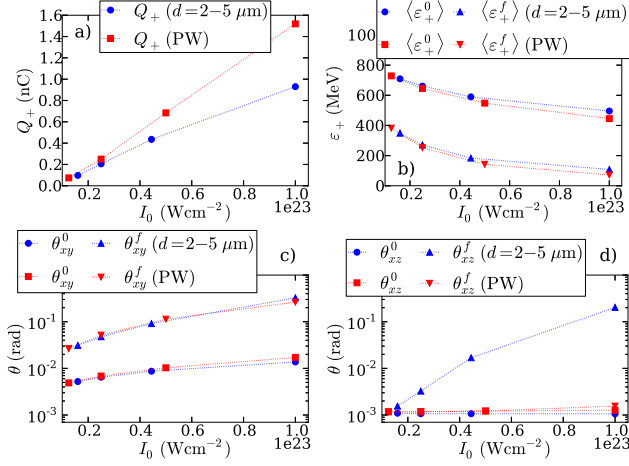


FIG. 4. Laser intensity dependence of the total positron charge (a), average energy (b) and divergence in the polarization (c) and perpendicular (d) planes at creation time (square and down triangle markers) and at the end of the interaction (circle and up triangle markers), for a focused wave (blue) or a plane wave (PW, red).

sion simulations with the same laser duration and energy as above but with varying spot size ($d = 2, 3, 4$ and $5 \mu\text{m}$). The corresponding peak intensities are $I_0 = 10^{23}$, 4.4×10^{22} , 2.5×10^{22} and $1.6 \times 10^{22} \text{ Wcm}^{-2}$. To further assess the influence of the transverse field gradients, this set of simulations is complemented by four simulations employing a laser plane wave at intensities $I_0 = 10^{23}$, 5×10^{22} , 2.5×10^{22} and $1.25 \times 10^{22} \text{ Wcm}^{-2}$.

Figure 4(a) shows that, in the focused case, the total positron charge rises with the laser intensity, albeit at an increasingly slower rate owing to the dropping number of electrons experiencing a strong field. In the plane-wave case, the positron charge grows linearly as $Q_+ [\text{nC}] \sim 0.17 I_{22}$ (where I_{22} is the intensity in 10^{22} Wcm^{-2}). A less expected result (not shown) is that the number of γ -ray photons (of energies $> 2m_e c^2$) weakly varies in our range of intensities. This is due to the strong γ -ray emission occurring in the foot of high-intensity pulses, which results in important electron deceleration at the time of peak intensity, and therefore in the production of relatively low-energy photons on average. At lower intensities, radiative losses are diminished so that the γ -ray emission takes place over the whole pulse duration at $I_0 = 1.25 \times 10^{22} \text{ Wcm}^{-2}$. Higher intensities, however, augment the probability for lower-energy photons to decay into pairs and consequently boost the positron yield.

Somewhat surprisingly, Fig. 4(b) reveals that the average positron energy at birth decreases with the laser intensity as $\langle \varepsilon_+^0 \rangle [\text{MeV}] \sim 490 I_{22}^{-0.8}$ for both the focused and plane waves. As the intensity rises, low-energy photons can more easily decay into pairs, thus enhancing

the number of low-energy positrons and, correspondingly, lowering the average positron energy. Furthermore, during their subsequent interaction with the laser field, the positrons radiate a larger fraction of their energy at higher intensities: from 48 % at $1.25 \times 10^{22} \text{ Wcm}^{-2}$ to 84 % at 10^{23} Wcm^{-2} for a plane wave. This effect further contributes to the decrease in the final mean positron energy with laser intensity.

The intensity dependence of the positron angular spread in the polarization and perpendicular planes is depicted in Figs. 4(c,d). In the xy polarization plane, the angular spreads in the focused and plane-wave regimes present a similar increase with intensity (from $\theta_{+,xy}^f \sim 0.025 \text{ rad}$ at $I_0 = 1.5 \times 10^{22} \text{ Wcm}^{-2}$ to $\sim 0.3 \text{ rad}$ at $I_0 = 10^{23} \text{ Wcm}^{-2}$), which confirms that QED scattering prevails in the considered intensity range. Both regimes also lead to a similar rise in the divergence during the interaction (from $\theta_{+,xy}^0$ to $\theta_{+,xy}^f$). In the xz perpendicular plane, the divergence mostly stems from the transverse ponderomotive force. As a result, for a plane wave, the final angular spread, $\theta_{+,xz}^f$, stays close to the initial value. By contrast, $\theta_{+,xz}^f$ increases with narrowing focal spot and increasing intensity, up to a value close to $\theta_{+,xy}^f$ at $I_0 = 10^{23} \text{ Wcm}^{-2}$.

Non-collinear geometry - A non-collinear collision geometry ($\theta \neq 180^\circ$) is generally used in experiments to prevent the reflected light from damaging the optics. For a $3 \mu\text{m}$ laser focal spot and a $4.4 \times 10^{22} \text{ Wcm}^{-2}$ peak intensity, our simulations show that the total positron charge remains approximately unchanged ($Q_+ \approx 0.4 \text{ nC}$) when the collision angle varies from $\theta = 180^\circ$ to 150° . In the worst-case perpendicular collision ($\theta = 90^\circ$), the positron yield drops down to $Q_+ = 0.03 \text{ nC}$.

Conclusion - Using full-scale 3D PIC simulations, we have demonstrated that soon-to-be-operational, multi-PW, multi-beam lasers will enable all-optical, high-repetition-rate schemes for efficient Breit-Wheeler pair production, which was as yet only accessible to large-scale accelerators. Besides providing a fully self-consistent modeling of the problem, our work presents important guidelines for future experiments. Our study thus reveals that the positron yield and mean divergence (resp. mean energy) increase (resp. decreases) with rising laser intensity at fixed laser energy. In particular, we find that a high-energy ($\sim 400 \text{ MeV}$), low-divergence ($\sim 0.02 \text{ rad}$) positron beam of charge $\sim 0.05 \text{ nC}$ can be achieved using a moderately-intense ($\sim 10^{22} \text{ Wcm}^{-2}$) laser pulse focused to a $\sim 5 \mu\text{m}$ spot. Once magnetically segregated from the electrons, this beam could serve as an injector source in conventional or optical accelerators. Higher pulse intensities ($\sim 10^{23} \text{ Wcm}^{-2}$) are required for generating dense ($Q_+ \sim 1 \text{ nC}$, $n_+ \sim n_c$), quasi-neutral pair plasmas, at the expense, however, of an increased divergence ($\gtrsim 0.1 \text{ rad}$) and a reduced mean energy ($\sim 100 \text{ MeV}$).

Acknowledgements - The authors acknowledge support by the French Agence Nationale de la Recherche (LABEX PALM-ANR-10-LABX-39, ANR SILAMPA) and interesting discussions with S.C. Wilks, F. Amiranoff and P. Audebert. The simulations were performed using HPC resources at TGCC/CCRT (Grant No. 2013-052707). We acknowledge PRACE for awarding us access to TGCC/Curie (Grant No. 2014112576). We thank the CCRT Team for the helpful support.

* mathieu.lobet@cea.fr

† xavier.davoine@cea.fr

‡ laurent.gremillet@cea.fr

- [1] R. Ruffini, G. Vereshchagin, and S.-S. Xue. Electron-positron pairs in physics and astrophysics: From heavy nuclei to black holes. *Phys. Rep.*, 487:1–140, February 2010.
- [2] S. Corde, E. Adli, J. M. Allen, W. An, C. I. Clarke, C. E. Clayton, J. P. Delahaye, J. Frederico, S. Gessner, S. Z. Green, M. J. Hogan, C. Joshi, N. Lipkowitz, M. Litos, W. Lu, K. A. Marsh, W. B. Mori, M. Schmeltz, N. Vafaei-Najafabadi, D. Walz, V. Yakimenko, and G. Yocky. Multi-gigaelectronvolt acceleration of positrons in a self-loaded plasma wakefield. *Nature*, 524:442445, 2015.
- [3] F. Tuomisto and I. Makkonen. Defect identification in semiconductors with positron annihilation: Experiment and theory. *Rev. Mod. Phys.*, 85:1583–1631, Nov 2013.
- [4] P. Mészáros. Theories of Gamma-Ray Bursts. *Annual Review of Astronomy and Astrophysics*, 40:137–169, 2002.
- [5] A. M. Bykov and R. A. Treumann. Fundamentals of collisionless shocks for astrophysical application, 2. Relativistic shocks. *Astron. Astrophys. Rev.*, 19:42, August 2011.
- [6] H. Chen, S. C. Wilks, J. D. Bonlie, E. P. Liang, J. Myatt, D. F. Price, D. D. Meyerhofer, and P. Beiersdorfer. Relativistic Positron Creation Using Ultraintense Short Pulse Lasers. *Phys. Rev. Lett.*, 102(10):105001, March 2009.
H. Chen, F. Fiuza, A. Link, A. Hazi, M. Hill, D. Hoarty, S. James, S. Kerr, D. D. Meyerhofer, J. Myatt, J. Park, Y. Sentoku, and G. J. Williams. Scaling the Yield of Laser-Driven Electron-Positron Jets to Laboratory Astrophysical Applications. *Phys. Rev. Lett.*, 114(21):215001, May 2015.
- [7] G. Sarri, K. Poder, J.M. Cole, W. Schumaker, A. Di Piazza, B. Reville, T. Dzelzainis, D. Doria, L. A. Gizzi, G. Grittani, S. Kar, C. H. Keitel, K. Krushelnick, S. P. D. Kuschel, Z. Mangles, Z. Najmudin, N. Shukla, L. O. Silva, D. Symes, A.G.R. Thomas, M. Vargas, J. Vieira, and M. Zepf. Generation of a neutral, high-density electron-positron plasma in the laboratory. *Nat. Comm.*, 6:6747, 2015.
- [8] B. Shen and J. Meyer-ter Vehn. Pair and γ -photon production from a thin foil confined by two laser pulses. *Phys. Rev. E*, 65:016405, Dec 2001.
- [9] A. R. Bell and J. G. Kirk. Possibility of prolific pair production with high-power lasers. *Phys. Rev. Lett.*, 101:200403, Nov 2008.
- [10] E. N. Nerush, I. Yu. Kostyukov, A. M. Fedotov, N. B. Narozhny, N. V. Elkina, and H. Ruhl. Laser field absorption in self-generated electron-positron pair plasma. *Phys. Rev. Lett.*, 106:035001, Jan 2011.
- [11] O. J. Pike, F. Mackenroth, E. G. Hill, and S. J. Rose. A photon-photon collider in a vacuum hohlraum. *Nature Photonics*, 8:434–436, June 2014.
- [12] CILEX, Centre Interdisciplinaire Lumière Extrême. <http://cilexsaclay.fr>.
- [13] ELI, extreme light infrastructure. <http://www.eli-beams.eu>.
- [14] A. Di Piazza, C. Müller, K. Z. Hatsagortsyan, and C. H. Keitel. Extremely high-intensity laser interactions with fundamental quantum systems. *Rev. Mod. Phys.*, 84:1177–1228, Aug 2012.
- [15] C. P. Ridgers, C. S. Brady, R. Ducloux, J. G. Kirk, K. Bennett, T. D. Arber, A. P. L. Robinson, and A. R. Bell. Dense electron-positron plasmas and ultraintense γ rays from laser-irradiated solids. *Phys. Rev. Lett.*, 108:165006, Apr 2012.
- [16] C. S. Brady, C. P. Ridgers, T. D. Arber, A. R. Bell, and J. G. Kirk. Laser absorption in relativistically underdense plasmas by synchrotron radiation. *Phys. Rev. Lett.*, 109(24):245006, 2012.
- [17] N.B. Narozhny, S.S. Bulanov, V.D. Mur, and V.S. Popov. On e^+e^- pair production by colliding electromagnetic pulses. *Journal of Experimental and Theoretical Physics Letters*, 80(6):382–385, 2004.
- [18] S.S. Bulanov, T.Zh. Esirkepov, A.G.R. Thomas, J.K. Koga, and S.V. Bulanov. Schwinger limit attainability with extreme power lasers. *Phys. Rev. Lett.*, 105(22):220407, 2010.
- [19] Yuan-Bin Wu and She-Sheng Xue. Nonlinear Breit-Wheeler process in the collision of a photon with two plane waves. *Phys. Rev. D*, 90(1):013009, 2014.
- [20] S.V. Bulanov, T.Zh. Esirkepov, Y. Hayashi, M. Kando, H. Kiriya, J.K. Koga, K. Kondo, H. Kotaki, A.S. Pirozhkov, S.S. Bulanov, et al. On the design of experiments for the study of extreme field limits in the interaction of laser with ultrarelativistic electron beam. *Nuclear Instruments and Methods in Physics Research Section A: Accelerators, Spectrometers, Detectors and Associated Equipment*, 660(1):31–42, 2011.
- [21] K. Tuchin. Non-linear pair production in scattering of photons on ultra-short laser pulses at high energy. *Phys. Lett. B*, 686(1):29 – 35, 2010.
- [22] I. V. Sokolov, N. M. Naumova, J. A. Nees, and G. A. Mourou. Pair creation in QED-strong pulsed laser fields interacting with electron beams. *Phys. Rev. Lett.*, 105:195005, Nov 2010.
- [23] S.S. Bulanov, C.B. Schroeder, E. Esarey, and W.P. Lee-mans. Electromagnetic cascade in high-energy electron, positron, and photon interactions with intense laser pulses. *Physical Review A*, 87(6):062110, 2013.
- [24] D. L. Burke, R. C. Field, G. Horton-Smith, J. E. Spencer, D. Walz, S. C. Berridge, W. M. Bugg, K. Shmakov, A. W. Weidemann, C. Bula, K. T. McDonald, E. J. Prebys, C. Bamber, S. J. Boege, T. Koffas, T. Kotseroglou, A. C. Melissinos, D. D. Meyerhofer, D. A. Reis, and W. Ragg. Positron production in multiphoton light-by-light scattering. *Phys. Rev. Lett.*, 79:1626–1629, Sep 1997.
- [25] A. Hartin, S. Porto, and G. Moortgat-Pick. Testing nonlinear-QED at the future linear collider with an intense laser. *arXiv preprint arXiv:1404.0810*, 2014.

- [26] F. Mackenroth and A. Di Piazza. Nonlinear Compton scattering in ultrashort laser pulses. *Phys. Rev. A*, 83:032106, Mar 2011.
- [27] N. Neitz and A. Di Piazza. Stochasticity effects in quantum radiation reaction. *Phys. Rev. Lett.*, 111:054802, Aug 2013.
- [28] M. Vranic, J. L. Martins, J. Vieira, R. A. Fonseca, and L. O. Silva. All-optical radiation reaction at 10^{21} W/cm². *Phys. Rev. Lett.*, 113:134801, Sep 2014.
- [29] T. G. Blackburn, C. P. Ridgers, J. G. Kirk, and A. R. Bell. Quantum radiation reaction in laser-electron-beam collisions. *Phys. Rev. Lett.*, 112:015001, Jan 2014.
T. G. Blackburn. Measuring quantum radiation reaction in laser-electron-beam collisions. *Plasma Phys. Control. Fus.*, 57(7):075012, 2015.
- [30] C. Harvey, M. Marklund, and E. Wallin. High-energy gamma-ray beams from nonlinear Thomson and Compton scattering in the ultra-intense regime. In *SPIE Optics+ Optoelectronics*, pages 950908–950908. International Society for Optics and Photonics, 2015.
- [31] G. Sarri, D.J. Corvan, W. Schumaker, J.M. Cole, A. Di Piazza, H. Ahmed, C. Harvey, C.H. Keitel, K. Krushelnick, S.P.D. Mangles, et al. Ultrahigh brilliance multi-MeV γ -ray beams from nonlinear relativistic thomson scattering. *Phys. Rev. Lett.*, 113(22):224801, 2014.
- [32] N. V. Elkina, A. M. Fedotov, I. Yu. Kostyukov, M. V. Legkov, N. B. Narozhny, E. N. Nerush, and H. Ruhl. QED cascades induced by circularly polarized laser fields. *Phys. Rev. ST Accel. Beams*, 14:054401, May 2011.
- [33] M. Lobet, E. d’Humières, M. Grech, C. Ruyer, X. Davoine, and L. Gremillet. Modeling of radiative and quantum electrodynamics effects in pic simulations of ultra-relativistic laser-plasma interaction. *arXiv preprint arXiv:1311.1107*, 2013.
- [34] W. Lu, M. Tzoufras, C. Joshi, F. S. Tsung, W. B. Mori, J. Vieira, R. A. Fonseca, and L. O. Silva. Generating multi-GeV electron bunches using single stage laser wake-field acceleration in a 3D nonlinear regime. *Phys. Rev. ST Accel. Beams*, 10:061301, Jun 2007.
- [35] A. F. Lifschitz, X. Davoine, E. Lefebvre, J. Faure, C. Réchatin, and V. Malka. Particle-in-cell modelling of laser-plasma interaction using Fourier decomposition. *J. Comp. Phys.*, 228(5):1803 – 1814, 2009.
- [36] E. Lefebvre et al. Electron and photon production from relativistic laser-plasma interactions. *Nuclear Fusion*, 43:629–633, July 2003.
- [37] H. Y. Wang, X. Q. Yan, and M. Zepf. Signatures of quantum radiation reaction in laser-electron-beam collisions. *Phys. Plasmas*, 22(9):093103, 2015.
- [38] S. R. Yoffe, Y. Kravets, A. Noble, and D. A. Jaroszynski. Longitudinal and transverse cooling of relativistic electron beams in intense laser pulses. *New Journal of Physics*, 17(5):053025, 2015.